34th Annual International Conference of the IEEE EMBS
San Diego, California USA, 28 August - 1 September, 2012

Stimulation Strength and Focality of Electroconvulsive Therapy with Individualized Current Amplitude: A Preclinical Study

Won Hee Lee, *Student Member, IEEE*, Sarah H. Lisanby, Andrew F. Laine, *Fellow, IEEE*, and Angel V. Peterchev, *Member, IEEE*

***Abstract*—This study investigates the stimulation strength and focality of electroconvulsive therapy (ECT) with individualized current amplitude in a nonhuman primate (NHP) model. We generated an anatomically realistic finite element model of a NHP head incorporating tissue heterogeneity and white matter conductivity anisotropy based on structural magnetic resonance imaging (MRI) and diffusion tensor MRI data. The electric field spatial distributions of three conventional ECT electrode placements (bilateral, bifrontal, and right unilateral) and an experimental frontomedial electrode configuration were simulated. We calibrated the electric field maps relative to an empirical neural activation threshold and evaluated the stimulation strength and focality of the various ECT electrode configurations with individualized current amplitudes corresponding to the motor threshold and seizure threshold assessed in the anesthetized NHP. Understanding the stimulation strength and focality of various forms of ECT could provide insight into the mechanisms of therapeutic seizure induction, and could provide support for the clinical investigation of ECT with individualized current amplitude as an intervention with potentially improved risk/benefit ratio.**

I. Introduction

ELECTROCONVULSIVE therapy (ECT) is a therapeutic intervention that induces a generalized seizure in anesthetized patients by administering electric current to the brain via scalp electrodes [1]. While ECT is an effective treatment for medication-resistant psychiatric disorders such as major depression, its adverse side effects (mostly amnesia [2]) limit its use. The antidepressant efficacy and cognitive side effects of ECT depend strongly upon the electrode configuration [3] and stimulus current characteristics including the degree to which the electric stimulus exceeds the threshold for seizure induction [4]. The tolerability of ECT can be improved by altering the placement or shape of the stimulating electrodes, for the purpose of controlling the induced electric field (E-field) distribution. For example, high dose right unilateral (RUL) ECT has a comparable efficacy to bilateral frontotemporal (BL) ECT with a significant decrease in amnesia [5]. Bifrontal (BF) and an investigational frontomedial (FM) configuration have been proposed to preferentially focus the E-field in prefrontal regions to maximize efficacy and limit side effects. We have argued for reduction and individualization of the stimulus current amplitude as a potential means of reducing side effects and clinical outcome variability [4, 6, 7]. However, the capability of these paradigms to focus the E-field has not been demonstrated directly.

Knowledge about the strength and spatial distribution of the E-field induced by ECT may help to unravel the mechanisms determining the efficacy and side effects seen with various ECT paradigms, and may inform novel techniques for improvement of spatial targeting of ECT which could lead to improved risk/benefit ratio [8]. However, the E-field alone is insufficient to predict the strength of neural stimulation, since the neural response is also dependent on other parameters such as the pulse shape and width [4, 9]. To overcome this limitation, we proposed previously, using a spherical head model, an E-field model incorporating a waveform-specific neural activation threshold to determine the suprathreshold direct stimulation strength and volume (focality) in ECT [9]. The spherical model, however, cannot account for detailed anatomical tissue features, individually variable head geometries, and anisotropic tissue properties. Furthermore, that study used a neural activation threshold estimated from the literature. Nonhuman primate (NHP) models of ECT are valuable for optimizing ECT technique [10] and can be used to empirically estimate the neural activation threshold.

In this study, we simulate the E-field distribution induced by ECT with an anatomically realistic finite element NHP head model. We estimate the neural activation threshold from the motor threshold (MT) and calibrate the simulated E-field maps relative to this threshold. We evaluate the stimulation strength and focality relative to the neural activation threshold for various ECT electrode configurations with individualized current amplitudes corresponding to the MT and amplitude-titrated seizure threshold (ST).

II. Methods

A. Structural and Diffusion Tensor MRI Acquisition

All studies were approved by the Duke University Institutional Animal Care and Use Committee. A healthy 11 year old male rhesus macaque (*Macaca mulatta*) underwent T1-weighted magnetic resonance imaging (MRI)

Manuscript received March 29, 2012; revised June 7, 2012. This work was supported by NIH grant R01MH091083.

W. H. Lee is with the Department of Biomedical Engineering, Columbia University, New York, NY 10027 and with the Department of Psychiatry and Behavioral Sciences, Duke University, Durham, NC 27710, USA (e-mail: wl2324@columbia.edu).

S. H. Lisanby is with Department of Psychiatry and Behavioral Sciences, and Department of Psychology & Neuroscience, Duke University, Durham, NC 27710, USA (e-mail: sarah.lisanby@duke.edu).

A. F. Laine is with the Department of Biomedical Engineering, Columbia University, New York, NY 10027, USA (e-mail: laine@columbia.edu).

A. V. Peterchev is with Departments of Psychiatry and Behavioral Sciences, Biomedical Engineering, and Electrical and Computer Engineering, Duke University, Durham, NC 27710, USA (phone: 919-684-0383; fax: 919-681-9962; e-mail: angel.peterchev@duke.edu).

(0.7×0.7×0.7 mm^3 voxel) and diffusion-weighted imaging (DWI) (1.4×1.4×1.4 mm^3 voxel). The subject was anesthetized with isoflurane during the scanning procedure. The MRI and DWI data were acquired on a Siemens 3 T Trio scanner using an 8-channel knee coil. The T1-weighted images were acquired with a 3D MPRAGE sequence [11]. The DWI scanning was performed in 12 non-collinear directions (b=1000 s/mm^2) with one non-diffusion weighted image using a single-shot spin-echo EPI sequence [11]. DWI acquisition was repeated six times and averaged. The DWI volumes were eddy-current corrected and diffusion tensors were estimated using FSL [12].

B. Finite Element Model Generation

The MRI images were upsampled to a resolution of 0.5×0.5×0.5 mm^3 and spatially aligned to the AC-PC coordinate system. The N4ITK algorithm [13] was applied to correct the MR image intensities for bias field inhomogeneity. Anisotropic diffusion filtering was then applied to reduce the image noise while preserving tissue boundaries [14]. We automatically extracted gray matter, white matter, and cerebrospinal fluid in SPM8 [15] based on the 112MR-SL macaque tissue priors [16]. The non-brain tissues were manually segmented into 11 subregions, including skin, muscle, compact bone, spongy bone, vertebrae, spinal cord, lens, eyeball, sclera, optic nerve, and sinus, using ITK-SNAP [17].

For finite element mesh generation, we used the restricted Delaunay tessellation algorithm [18], resulting in a finite element model of the rhesus macaque head and electrodes consisting of approximately 1.8 million tetrahedral elements.

C. Tissue Conductivity

All tissue compartments were considered electrically isotropic except the white matter tissue. To estimate the white matter conductivity anisotropy, we assumed that the conductivity tensors share eigenvectors with the measured diffusion tensors [19]. We then deployed the volume constraint technique with a fixed anisotropy ratio of 10:1 (parallel:transverse) in each white matter voxel. The tissue electric conductivity values are listed in Table I [8, 20, 21].

D. Electrode Configurations

We modeled three standard ECT electrode placements (BL, BF, and RUL) and an investigational configuration (FM). Two round electrodes were modeled for the BL (3.5 cm diameter) and BF, RUL, and FM (2.5 cm diameter, respectively) ECT configurations (see Fig. 1). For BL ECT, the two electrodes were placed bilaterally at the frontotemporal positions located at 2 cm above the midpoint of the line connecting the external canthus and tragus. For BF ECT, the electrodes were positioned bilaterally 2.5 cm above the outer angle of the orbit on a line parallel to the sagittal plane. For RUL ECT, one electrode was placed in the right frontotemporal position and the other electrode was centered 1.25 cm to the right of vertex. For FM ECT, the two electrodes were placed medially on the forehead and posterior to vertex, respectively.

TABLE I
TISSUE ELECTRICAL CONDUCTIVITIES

Tissue	Conductivity (S/m)	Tissue	Conductivity (S/m)
Skin	0.43	Spinal cord	0.15
Muscle	0.32	Vertebrae	0.012
Skull (compact bone)	0.0063	Lens	0.32
Skull (spongy bone)	0.04	Eyeball	0.5
Cerebrospinal fluid	1.79	Sclera	0.5
Gray matter	0.33	Optic nerve	0.14
White matter (parallel)	0.65	Sinus	0
White matter (transverse)	0.065	Electrode	9.8×10^5

E. Electric Field Simulation

The E-field distribution for all ECT electrode configurations was computed using the finite element method software ANSYS (ANSYS Inc., Canonsburg, PA, USA). Since the frequencies used in ECT are relatively low (< 10 kHz), the E-field solution was obtained by solving the quasi-static Laplace equation with no internal sources [8]

$$\nabla \cdot (\sigma \nabla V) = 0 \quad (1)$$

where V and σ denote the electric potential and the tissue electric conductivity tensor, respectively. For each of the electrode configurations, the induced E-field distribution inside the head was calculated using the preconditioned conjugate gradient solver within ANSYS.

F. In Vivo Motor and Seizure Threshold Titration

We determined the MT corresponding to the amplitude of a single pulse required to elicit a motor response, and the ST corresponding to the amplitude for a train of pulses to elicit a seizure in the same session for each of the ECT electrode configurations [7]. MT and ST were titrated by adjusting current amplitude (pulse width = 0.2 ms) in the anesthetized NHP. For MT, electromyography was measured from the first dorsal interosseous (FDI) muscle in both hands for all ECT conditions, but only from the left hand in the RUL ECT condition since the stimulation is predominantly unilateral in the right hemisphere. The MT was determined for both current polarities. The MT was defined as the minimum stimulus pulse amplitude needed to achieve a 50 μV peak-to-peak motor evoked potential for at least five out of ten trials.

ST was determined by an ascending method-of-limits titration of the stimulus pulse amplitude. All stimulus parameters besides the pulse amplitude were held constant. The stimulus train consisted of 500 pulses delivered at 50 pulses per second resulting in train duration of 10 s. ST titrations for BL and RUL ECT used unidirectional pulse trains (cathode on right side) whereas the ST titrations for BF and FM ECT used a conventional bidirectional train (alternating pulse polarity). Seizures were determined by observing the motor seizure manifestations in the left arm and the EEG as a secondary criterion.

G. Stimulation Strength and Focality

We derived an empirical estimate of the neural activation threshold from the median E-field in the FDI region of motor cortex at stimulation current corresponding to MT for RUL which produces E-field most localized to FDI. This estimate

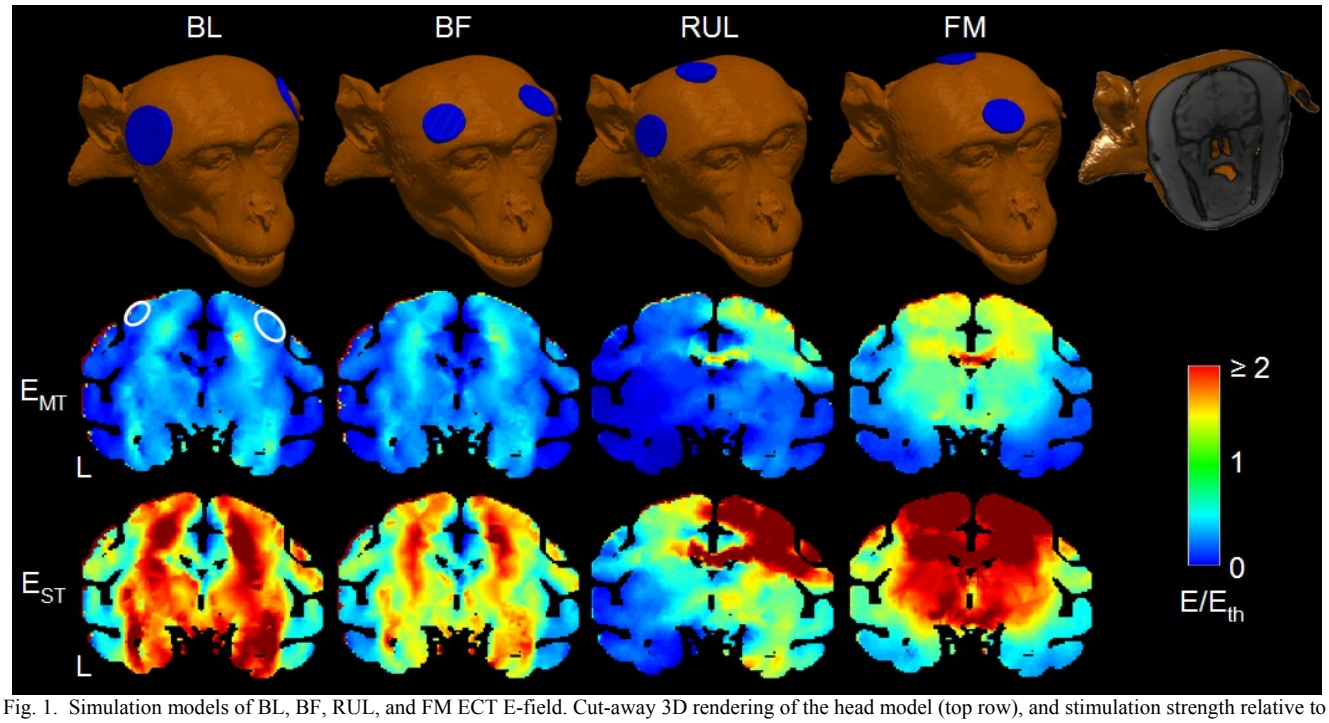

Fig. 1. Simulation models of BL, BF, RUL, and FM ECT E-field. Cut-away 3D rendering of the head model (top row), and stimulation strength relative to the threshold motor response (E_{MT}, middle row) and the threshold for inducing seizures (E_{ST}, bottom row) for BL, BF, RUL, and FM electrode configurations (left to right columns, respectively). E_{th}: threshold E-field strength (0.3 V/cm for a pulse width of 0.2 ms). Region-of-interest (ROI) outlines in white show first dorsal interosseous (FDI) motor area. L: left.

was compared to an estimate derived from the literature, E_{th} = 0.29 V/cm for 0.2 ms pulse width [9]. The stimulation strength relative to threshold was then calculated by dividing the E-field by the threshold, E/E_{th}.

Using the current amplitudes corresponding to MT and ST, we computed corresponding E-field magnitude maps E_{MT} and E_{ST}. The stimulation focality was quantified by the percentage of the brain volume that is exposed to E-field strong enough to produce suprathreshold depolarization in the majority of neurons, i.e., the volume where $E/E_{th} \geq 1$ [9].

TABLE II
AVERAGE MOTOR THRESHOLD (MA) FOR LEFT (L) AND RIGHT (R) HANDS AND AVERAGE SEIZURE THRESHOLD (MA) FOR FOUR ECT ELECTRODE CONFIGURATIONS

Electrode Configuration	Average MT		Average ST
	L Hand	R Hand	
BL	41	41	111
BF	43	42	92
RUL	50	N/A	114
FM	47	49	89

III. RESULTS

Table II gives the empirical average MT for left and right hands and average ST values for the various electrode configurations. Average MT values in the left hand were used for computing the stimulation strength for each of the ECT electrode configurations. Based on the median E-field strength in the FDI area for RUL at MT, we estimated the neural activation threshold to be E_{th} = 0.32 V/cm, which is within 10% of the literature estimate of 0.29 V/cm.

Fig. 1 shows the four simulated ECT electrode montages (BL, BF, RUL, and FM) and representative E-field maps relative to the neural activation threshold at current strengths corresponding to MT and ST.

Fig. 2 (a) shows descriptive statistics on the E-field magnitude relative to neural activation threshold at MT and ST. The percentage of brain volume stimulated above threshold E_{th} is shown in Fig. 2 (b). BL and FM ECT produce the strongest median E-field at ST (0.33 V/cm). BL ECT stimulates the largest brain volume (61%) at ST, whereas RUL is the most focal (30% stimulated volume). FM ECT stimulates the largest brain volume at MT (17%) and close to the largest volume at ST (59%).

IV. DISCUSSION AND CONCLUSIONS

We investigated the E-field stimulation strength and focality of various ECT electrode configurations with individualized current amplitudes using a realistic NHP head model and empirical MT and ST data. The results in Fig. 1 demonstrate that different ECT configurations result in substantially different E-field characteristics in the brain even when the current strength is at the lowest level required to activate the corticospinal tract (MT) or to induce a seizure (ST). We also found that the median E-field in FDI motor area determined from the most focal stimulation (RUL) with current amplitude corresponds to the individual MT, consistent with published estimates of threshold E-field strength, indirectly supporting the validity of our model. Thus, our study illustrates the utility of the physiologically-calibrated computational E-field model to analyze various stimulus delivery paradigms, and may inform improved ECT technique with individually-titrated dosage.

Our data shows that seizure induction with a combination of a relatively focal electrode configuration (RUL) and individually titrated current (ST) results in an E-field distribution

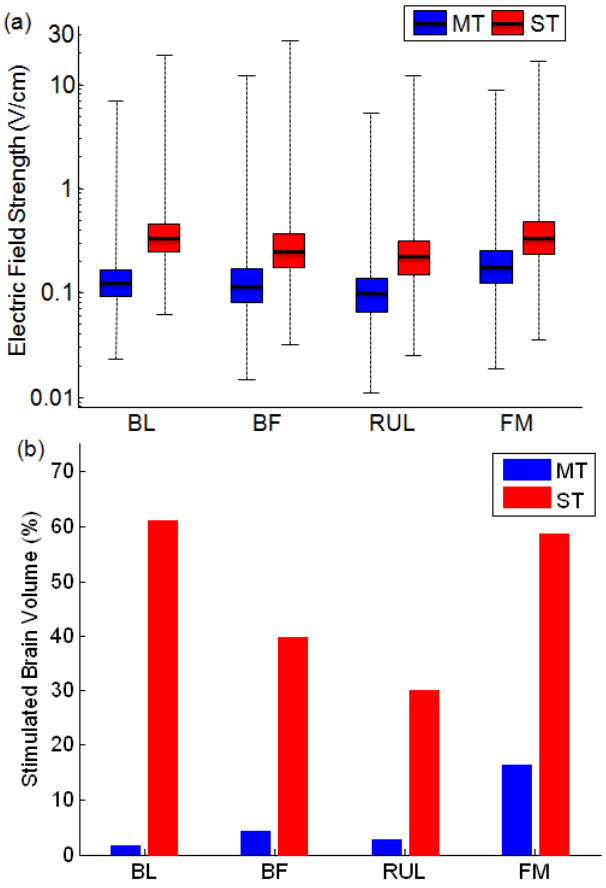

Fig. 2. (a) Descriptive statistics of E-field magnitude relative to neural activation threshold at MT and ST. The E-field strength (y-axis) is shown on a logarithmic scale. The boxes indicate the interquartile range (25th to 75th percentile) with the median marked by a thick horizontal black line. The whiskers delimit the minimum and maximum of the E-field distribution. (b) Percentage brain volume stimulated above threshold ($E \geq E_{th}$).

with magnitude below the neural activation threshold in 70% of the brain. This suggests the regions of the brain that may be critical to cognitive side effects such as the left temporal lobe may be spared, since the E-field strength there is well below the neural activation threshold (see Fig. 1). On the other hand, the robust therapeutic effectiveness of BL ECT may stem from the relatively even spread of the E-field and associated large volume of stimulated brain tissue even at ST.

The experimental FM configuration stimulated a large brain volume at both MT and ST. This may indicate that the E-field has to be strong enough to reach the motor strip even when the electrodes are focused away from the motor strip.

These observations may provide rational basis for future clinical studies with various electrode placements and individualized current amplitude.

V. Acknowledgement

The authors thank Mohamed Aly, Brian Chan, Niko Reyes, Moacyr A. Rosa, Christopher Sikes-Keilp, and Nagy Youssef for assisting in the NHP procedures and data entry.

VI. References

[1] R. Abrams, *Electroconvulsive therapy*, 4th Ed. New York: Oxford Unversity Press, 2002.

[2] H. A. Sackeim, J. Prudic, R. Fuller, J. Keilp, P. W. Lavori, and M. Olfson, "The cognitive effects of electroconvulsive therapy in community settings," *Neuropsychopharmacology,* vol. 32, pp. 244-254, 2007.

[3] C. H. Kellner, K. G. Tobias, and J. Wiegand, "Electrode placement in electroconvulsive therapy (ECT): A review of the literature," *J. ECT,* vol. 26, pp. 175-180, 2010.

[4] A. V. Peterchev, M. A. Rosa, Z. D. Deng, J. Prudic, and S. H. Lisanby, "Electroconvulsive therapy stimulus parameters: rethinking dosage," *J. ECT,* vol. 26, pp. 159-174, 2010.

[5] H. A. Sackeim, J. Prudic, D. P. Devanand, M. S. Nobler, S. H. Lisanby, S. Peyser, L. Fitzsimons, B. J. Moody, and J. Clark, "A prospective, randomized, double-blind comparison of bilateral and right unilateral electroconvulsive therapy at different stimulus intensities," *Arch. Gen. Psychiatry,* vol. 57, pp. 425-434, 2000.

[6] M. A. Rosa, G. L. Abdo, S. H. Lisanby, and A. V. Peterchev, "Seizure induction with low-amplitude-current (0.5A) electroconvulsive therapy," *J. ECT,* vol. 27, pp. 341-342, 2011.

[7] A. V. Peterchev, B. Chan, and S. H. Lisanby, "Pulse amplitude adjustment: a novel means of individualizing and predicting dosage requirements for electroconvulsive therapy and magnetic seizure therapy," *J. ECT,* vol. 26, p. 154, 2010.

[8] W. H. Lee, Z. D. Deng, T. S. Kim, A. F. Laine, S. H. Lisanby, and A. V. Peterchev, "Regional electric field induced by electroconvulsive therapy in a realistic finite element head model: influence of white matter anisotropic conductivity," *NeuroImage,* vol. 59, pp. 2110-2123, 2012.

[9] Z. D. Deng, S. H. Lisanby, and A. V. Peterchev, "Electric field strength and focality in electroconvulsive therapy and magnetic seizure therapy: a finite element simulation study," *J. Neural Eng.,* vol. 8, 2011.

[10] S. H. Lisanby, T. Moscrip, O. Morales, B. Luber, C. Schroeder, and H. A. Sackeim, "Neurophysiological characterization of magnetic seizure therapy (MST) in non-human primates," *Suppl. Clin. Neurophysiol.,* vol. 56, pp. 81-99, 2003.

[11] X. Liu, T. Zhu, T. Gu, and J. Zhong, "A practical approach to in vivo high-resolution diffusion tensor imaging of rhesus monkeys on a 3-T human scanner," *Mag. Resonance Imaging,* vol. 27, pp. 335-346, 2009.

[12] S. M. Smith, M. Jenkinson, M. W. Woolrich, C. F. Beckmann, T. E. Behrens, H. Johansen-Berg, P. R. Bannister, M. De Luca, I. Drobnjak, D. E. Flitney, R. K. Niazy, J. Saunders, J. Vickers, Y. Zhang, N. De Stefano, J. M. Brady, and P. M. Matthews, "Advances in functional and structural MR image analysis and implementation as FSL," *NeuroImage,* vol. 23 Suppl 1, pp. S208-219, 2004.

[13] N. J. Tustison, B. B. Avants, P. A. Cook, Y. Zheng, A. Egan, P. A. Yushkevich, and J. C. Gee, "N4ITK: improved N3 bias correction," *IEEE Trans. Med. Imaging,* vol. 29, pp. 1310-1320, 2010.

[14] W. H. Lee, T. S. Kim, M. H. Cho, Y. B. Ahn, and S. Y. Lee, "Methods and evaluations of MRI content-adaptive finite element mesh generation for bioelectromagnetic problems," *Phys. Med. Biol.,* vol. 51, pp. 6173-6186, 2006.

[15] J. Ashburner and K. J. Friston, "Unified segmentation," *NeuroImage,* vol. 26, pp. 839-851, 2005.

[16] D. G. McLaren, K. J. Kosmatka, T. R. Oakes, C. D. Kroenke, S. G. Kohama, J. A. Matochik, D. K. Ingram, and S. C. Johnson, "A population-average MRI-based atlas collection of the rhesus macaque," *NeuroImage,* vol. 45, pp. 52-59, 2009.

[17] P. A. Yushkevich, J. Piven, H. C. Hazlett, R. G. Smith, S. Ho, J. C. Gee, and G. Gerig, "User-guided 3D active contour segmentation of anatomical structures: significantly improved efficiency and reliability," *NeuroImage,* vol. 31, pp. 1116-1128, 2006.

[18] J. P. Pons, E. Segonne, J. D. Boissonnat, L. Rineau, M. Yvinec, and R. Keriven, "High-quality consistent meshing of multi-label datasets," *Inf. Process. Med. Imaging,* vol. 20, pp. 198-210, 2007.

[19] P. J. Basser, J. Mattiello, and D. Lebihan, "MR Diffusion Tensor Spectroscopy and Imaging," *Biophy. J.,* vol. 66, pp. 259-267, 1994.

[20] J. Haueisen, C. Ramon, M. Eiselt, H. Brauer, and H. Nowak, "Influence of tissue resistivities on neuromagnetic fields and electric potentials studied with a finite element model of the head," *IEEE Trans. Biomed. Eng.,* vol. 44, pp. 727-735, 1997.

[21] R. J. Sadleir, T. D. Vannorsdall, D. J. Schretlen, and B. Gordon, "Transcranial direct current stimulation (tDCS) in a realistic head model," *NeuroImage,* vol. 51, pp. 1310-1318, 2010.